Stochastic Methods to Predict WEC Array Power for Grid Integration

Helen Bailey[1], Bryson Robertson, Juan Ortiz, Bradley Buckham
Mechanical Engineering Department, University of Victoria
BC, Canada
[1]hlbailey@uvic.ca

Abstract— **The temporal characteristics of power output from large arrays of wave energy converters (WECs) needs to be quantified prior to large scale electrical grid integration. Using detailed numerical modelling techniques, this study develops a novel stochastic model allowing for the rapid prediction of WEC array power, based on the known power output time series of a single WEC simulation.**

The study spatially distributes up to 250 individual WEC's within a numerical test bed and accurately aggregates the power time series. The time variation of the power recovered from the numerical WEC arrays has been systematically analysed to determine the effect of different WECs designs, different sea-states and different directional wave spreading functions. Noting that individual WEC designs produce power from fundamentally different wave motions, 4 different WEC concepts are considered in the development of the stochastic models.

Through analysis of the WEC power standard deviation and frequency domain spectrum, using knowledge of both a single WEC and an array of WECs, a stochastic model of WEC array power production has been developed and validated.

As the wave energy industry matures, detailed models of WEC array power output will necessary to ensure the feasibility of future electrical grid integration and allow for high wave energy penetration.

***Keywords*— Arrays, Wave Energy Converters, power quality, electricity grid integration**

I. Introduction

The temporal characteristics of power output from large arrays of WECs needs to be quantified prior to large scale electrical grid integration. The power output from WEC arrays have been considered by many previous authors, typically for a single WEC concept with arrays of between 3 and 50 units [1]–[6]. This work builds on these studies by introducing a novel method of predicting WEC array power, based on a stochastic model of a single device. Utilizing detailed numerical modelling techniques, this study spatially distributes up to 250 individual WEC's within a numerical test bed and accurately aggregates the time power series, to enable the development of the stochastic model.

In order investigate the model applicability across differing WEC designs, this study uses detailed knowledge of 4 different WEC concepts, each with inherently different operational characteristics and power production concepts. The four diverse WECs considered have been chosen based on their differences: differences in energy recovery concepts; differences in rated power, differences in deployment depths and spatial distribution.

In this paper, Section II provides an overview of the numerical simulation; providing details of the different WEC's, the different methods used to model them and their individual array design. The results of the simulations are presented in Section III along with a statistical and frequency domain analysis. The stochastic model is introduced in Section IV, and discussions are presented in Section V. The paper is concluded in Section VI.

II. Numerical Simulation

A. The WECs

The WECs used in this study are briefly described below. Table I provides an overview of the forces acting on each of the WECs and the different simulation methods used to model the WECs. For interested readers, each section provides references for further detail.

1) *Backwards Bent Duct Buoy (BBDB)*: The BBDB is a floating Oscillating Water Column WEC [7], [8], with a 17.5 m draft, a 27 m beam and a 35 m length. For modelling purposes, it is simulated as a two body system; a floating structure and a separate light piston. The light piston represents the surface of the water within the air chamber. The hydrodynamic wave forcing is experienced by both of these bodies, while their individual motions induce coupled and cross coupled radiation forces. The air chamber thermodynamics are simulated in order to track the volume, pressure, density and air flow though the turbine. The associated relative internal pressure exerts a force on both bodies. The BBDB Power Take Off (PTO) is modelled as a Variable Radius Turbine (VRT), with a constant rotational speed. The BBDB has a 3 point mooring system, with floater and sinker buoys positioned on its aft line. Further details of the BBDB and how it was simulated are available in [9]. An image of the BBDB is presented in Figure 1.

2) *Resolute Marine Energy (RME):* RME is developing an 8 m wide, shallow water surging flap WEC [10]. The surging flap operates in near shore locations to minimize distances, and associated expenses, to either the electricity grid nodes or off-grid communities. The buoyant flap rotates about a fixed axis, which is rigidly attached to the seabed (see Figure 2). A hydraulic cylinder operates between the flap and the fixed

base. The motion of the flap compresses and expands the hydraulic cylinder pumping a working fluid to shore [11].

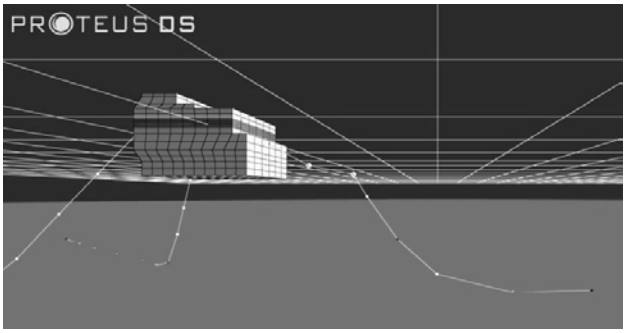

Fig. 1 The BBDB WEC, shown in the ProteusDS environment

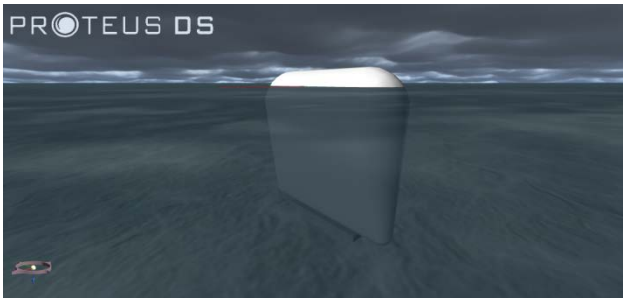

Fig. 2 Schematic drawing of RME's flap WEC

3) *SurfPower*: SurfPower is a surface following float being developed by Seawood Designs. SurfPower is a buoyant rectangular pontoon that floats on the water surface and is free to move in 5 degrees of freedom (see Figure 3). In simulation, the device is locked in yaw due to a proprietary yaw control mechanism that is planned for real-world deployments. The buoyant float has dimensions of 24 m long, 7 m wide and a depth of 1 m. The pontoon is attached to a hydraulic cylinder via a static bridle. The hydraulic cylinder is attached at its base to the ocean floor and it is able to rotate around this fixed point. In the simulations a water depth of 40 m is assumed. As the pontoon moves, the hydraulic cylinder expands and contracts. Power is extracted only on the upstroke of the hydraulic piston [11]–[13].

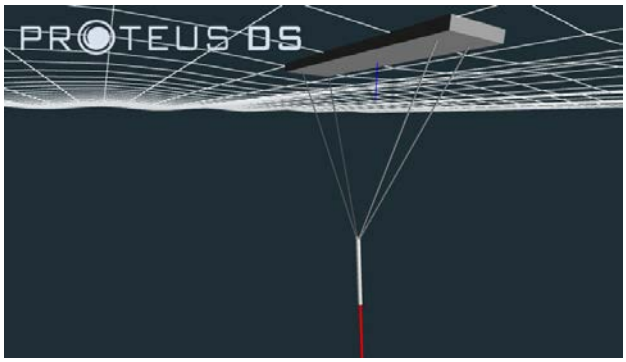

Fig. 3 SurfPower shown in the ProteusDS environment

3) *Two-body Point Absorber (2B-PA):* The University of Victoria maintains an axisymmetric two body WEC, which features a circular cylinder buoyant float, with a 15 m diameter, co-axially aligned with a 39 m tall spar (see Figure 4). The spar is free to move in 6 degrees of freedom while the float can only move along the co-axial axis of the spar. A viscous PTO operates between the two bodies and the power is extracted for both directions of relative movement. The system is slack moored to the seabed. This concept is designed as a research platform for the University of Victoria rather than a commercial concept [14], [15].

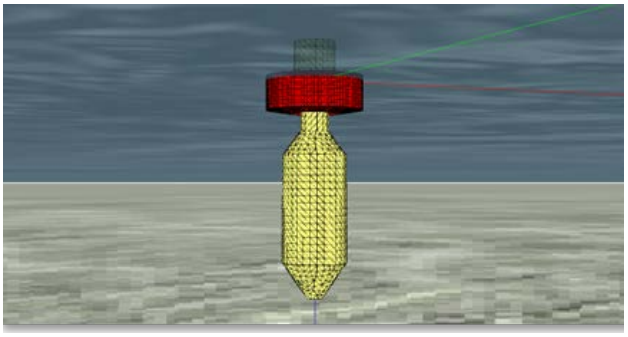

Fig. 4 The 2B-PA, shown in the ProteusDS environment.

B. Modelling technique

The hydrodynamic motions of the WEC, and the associated forcing on the WEC's PTO, depend on the forces from the incident waves, forces induced by motions of the WECs (including moorings were appropriate) and forces from the PTO. These forces are discussed below and a summary of the simulation inputs for each WEC type are presented in Table I.

1) *Excitation Force*: The excitation force is the summation of the dynamic pressures across the body, from both the incoming and diffracted waves [16]. The excitation forces can be obtained directly from WAMIT, when the body is stationary for different wave frequencies and directions, or by using the undisturbed incoming wave field and summing the dynamic pressures across the wetted panels of WEC in the current position of the body.

2) *Radiation force*: The radiation forces result from the motion of the bodies in the fluid, without the presence of the incident waves. These are calculated in the time domain from the convolution of the velocity time history and the impulse response kernel built from WAMIT hydrodynamic radiation damping coefficients. These forces can also be assumed frequency independent and proportional to the current velocity.

3) *Buoyancy force:* The buoyancy force is calculated either from the position of the body and its hydrodynamic stiffness or by the hydrostatic pressure across the submerged portion of the body from the undisturbed incident waves.

4) Mooring forces: Moorings forces are calculated using a finite-element cable model; specifically a cubic-spline lumped mass cable model [17]. The cable's material properties: the bending or flexural rigidity, the torsional rigidity and the axial rigidity are specified. The cable is discretised into a number of lumped masses connected by massless elastic elements. For each lumped mass, the forces

TABLE I
HYDRODYNAMIC PROPERTIES FOR THE NUMERICAL MODEL OF THE DIFFERENT WECS

	BBDB	RME	SurfPower	2B-PA
Excitation Force	Calculated from WAMIT for the main body and the piston, representing the water column height.	The excitation forces on the flap are obtained from WAMIT.	Froude-Krylov force is calculated from the absolute position of the pontoon and the dynamic pressure of the undisturbed wave field.	The excitation forces on the float and spar are obtained from WAMIT.
Radiation Force	Coupled radiation forces are calculated for 6 DOF for the BBDB body and for the heave of the piston. Cross coupled radiation forces are calculated for the piston heaving and the BBDB heaving, surging and pitching.	Radiation forces from the flaps motion are obtained from WAMIT.	A frequency independent damping force is used based on experimental testing	Radiation forces on the individual bodies are calculated based on WAMIT results. However, no cross coupled radiation forces are considered.
Buoyancy	A linear hydrostatic matrix for the BBDB body. Heave only for the piston.	A linear relation between buoyancy force and flap rotation	Nonlinear relation; dependant on whether the centroid of the mesh is wet from the undisturbed wave field.	A linear hydrostatic matrix based on the bodies' absolute position.
PTO	Thermodynamic model of the pressures within the air chamber providing air flow through a VRT.	Coulomb damper representing a hydraulic system.	Coulomb damper representing a hydraulic PTO which only operates on the upstroke of the piston.	A viscous damper with forces opposing and in proportion to the relative velocity.
Viscous Drag	External body and internal piston drag. Coefficients obtained from standard values	Coefficients obtained from scaled experiments on a similar shape.	Coefficients obtained from scaled experiments	Coefficients obtained from scaled experiments. No viscous drag on the float.

from the waves, forces from the neighbouring lumped masses or attached body or ground are calculated and used for the time progression [18].

5) *Power Take Off*: The PTO extracts power from the WEC. The 4 different WECs considered use very different types of PTO systems (see Table I). The PTO operates based on the relative motion of WEC components. For example, the relative motion between two bodies, the seabed or a volume of water.

6) *Viscous drag*: A "Morison's approach" is used to determine the viscous drag. Drag coefficients are used to calculate the drag force, which is proportional to the relative motion of the body and the neighbouring water particles, for translational degrees of freedom. For each considered WEC, different techniques have been used to obtain the viscous drag coefficients.

In order to maintain computational efficiency the hydrodynamic simulations do not include radiation effects from one WEC to another WEC in the array. Nor do they include any changes in the wave field due to the presence of the other WECs in the array. These effects are mitigated by keeping the number of rows low relative to the number of columns, and by having large column spacing and row offsets (see Figure 5 and Table II). It is acknowledged that changes in the wave field will occur and an overall reduction in the amount of power recovered is not accounted for [19].

C. Array Design

Each WEC array has a rated capacity of 50 MW, which is considered to be a significant utility scale renewable energy generation source on Vancouver Island, Canada [20]. The exact number of WECs and positioning within the arrays varies depending on the size and overall seabed footprint of the different WEC architectures. The WECs are deployed in parallel rows, perpendicular to the primary wave direction. The WECs in the subsequent rows are offset from the WEC directly in front of them. A schematic plan of the array is presented in Figure 5 and WEC array parameters are presented in Table II. The 50 unit array has 5 rows and 10 columns of WECs; while the 250 unit array has 10 rows and 25 columns of WECs.

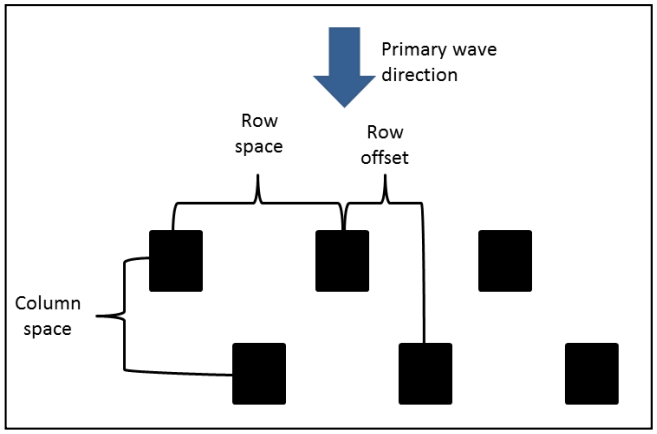

Fig. 5: Schematic view of the array layout

TABLE II
ARRAY SPACING AND DETAILS FOR THE DIFFERENT WECS

	BBDB	RME	Surf-Power	2B-PA
Row space	1200 m	25 m	100 m	200 m
Row offset	300 m	8.33 m	25 m	50 m
Column space	400 m	200 m	100 m	200 m
Total units for 50 MW farm	50	>250	250	250

III. ARRAY RESULTS

With the sole exception of the BBDB, each WEC was simulated in a both a 50 unit and 250 unit array. The arrays are simulated in the sea-states presented in Table III, defined by the significant wave heights (Hs) and the peak period (Tp) values for a JONSWAP spectrum. The sea-states chosen represent two high occurrence wave energy transport sea states for Amphitrite Bank, Vancouver Island, Canada [21]. The significant wave heights were reduced to 1.25 m and 0.875 m for the RME arrays given their shallow water near shore deployment location. The phases of the superimposed regular sinusoidal waves, used to create the irregular wave spectrum, were randomly generated for each scenario and for each WEC. The spread of the spectrum refers to the directional spread of the incoming wave field. The wave headings are ± 90 degrees from the primary wave direction. The amplitudes of the waves are multiplied by:

$$\left(\frac{\Gamma(1+0.5n)}{\sqrt{\pi}\Gamma(0.5+0.5n)}\cos^{n}(\theta-\theta_p)\right)^{0.5} \quad (1)$$

where Γ is the gamma function, θ is the direction of the individual wave and θ_p is the primary wave direction. n is the spread parameter that is varied in this work [22]. For the sea-states with a wide spread, either an n of 1 was used or a uniformly spread spectrum.

The simulations were run for 600 s, plus between 10 and 40 s to allow for the initial transients to decay. The power data has only been extracted for the final 600 s after the initial transients have decayed. This length of simulation time allows a large number of wave events to occur while limiting the computational time required.

TABLE III
THE DIFFERENT ARRAY SCENARIOS TESTED

Scenario	Hs	Tp	Spread description	*n*
1	2.75	10.5	Standard	2
2	1.75	8.85	Standard	2
3	2.75	10.5	Narrow	10
4	2.75	10.5	Wide	1 or uniform

A. *Array Power Recovered*

For scenario 1 (as per Table III), the power recovered from the array of WECs is summated to determine the total array power. The results for the different WECs are presented in Figure 6-9. The "Single WEC" line represents the power series determined by directly multiplying the power from a single WEC by the number of simulated devices, The "50/250 WEC Array" line represents the aggregation of the power series' from the numerical simulations.

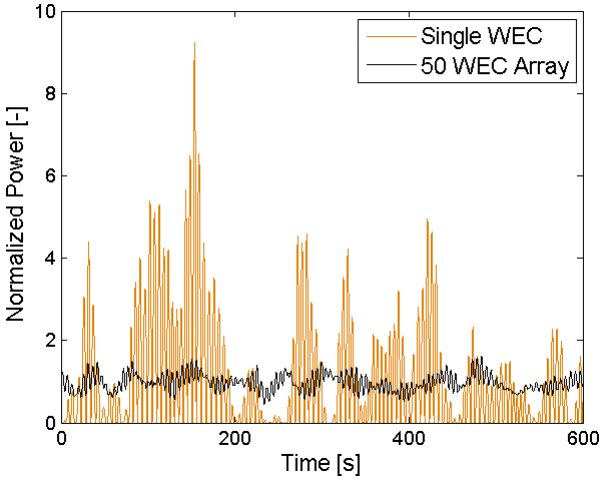

Fig. 6: The power from a single unit and an array of BBDB's

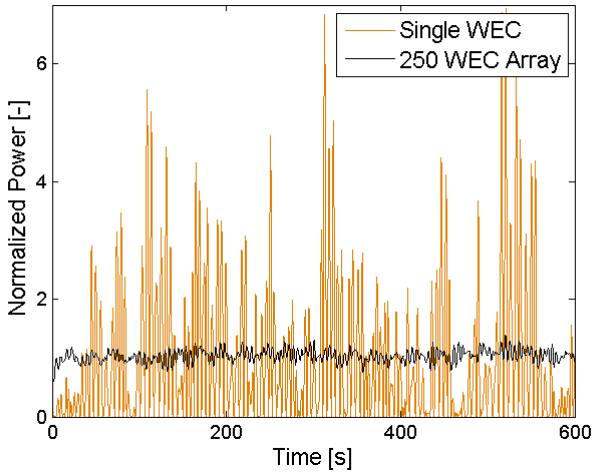

Fig. 7: The power from a single unit and an array of RME flaps

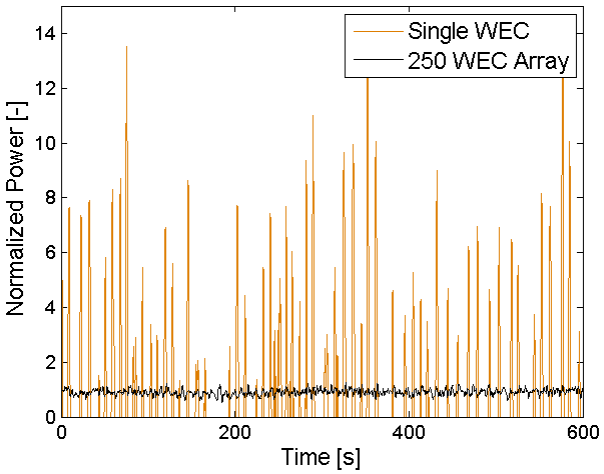

Fig. 8: The power from a single unit and an array of SurfPower's

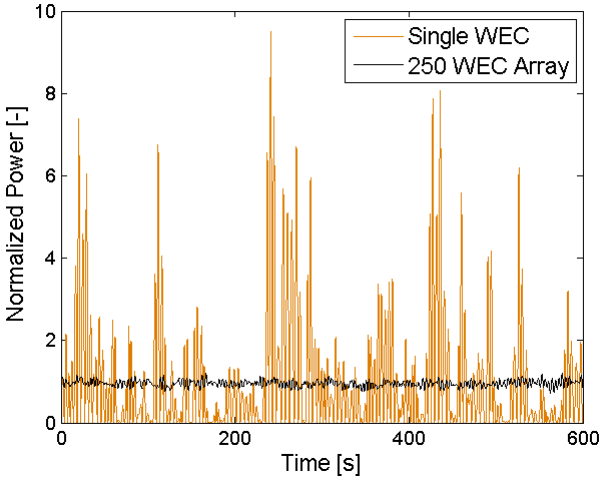

Fig. 9: The power from a single unit and an array of 2B-PA concepts

B. *Standard Deviation Array Ratio*

The Standard Deviation Array Ratio (SDAR) is introduced. The SDAR is defined as the standard deviation of the total power of the simulated array, divided by the standard deviation of the product of the power from a single unit and the number of units currently in the array (see equation 2).

$$SDAR = \frac{STD(array\ power)}{STD(1\ WEC\ \ power\ \times number\ of\ WECs)} \quad (2)$$

Presented in Figures 10-13 is the SDAR for varying numbers of units with the WEC arrays for the 4 different scenarios.

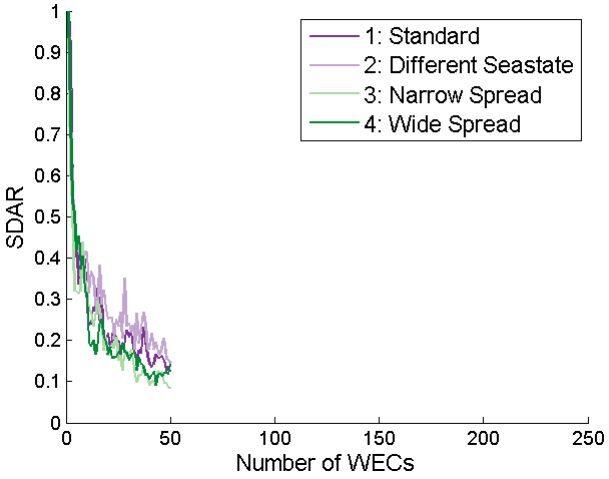

Fig. 10: SDAR's for an array of BBDB's

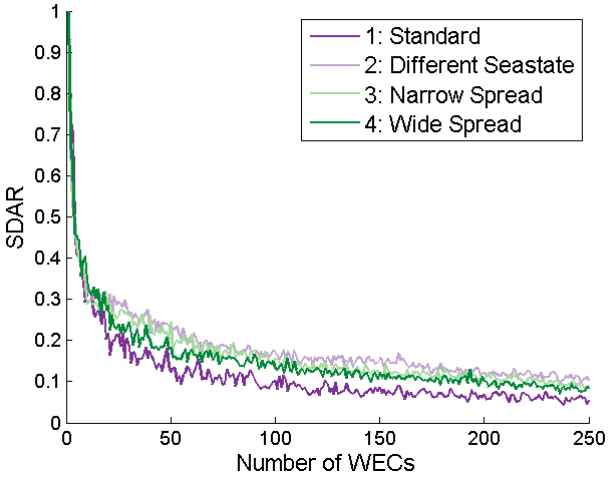

Fig. 11: SDAR's for an array of RME's flaps

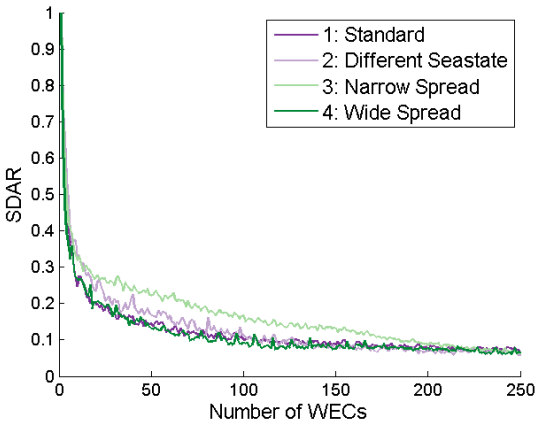

Fig. 12: SDAR's for an array of SurfPower units

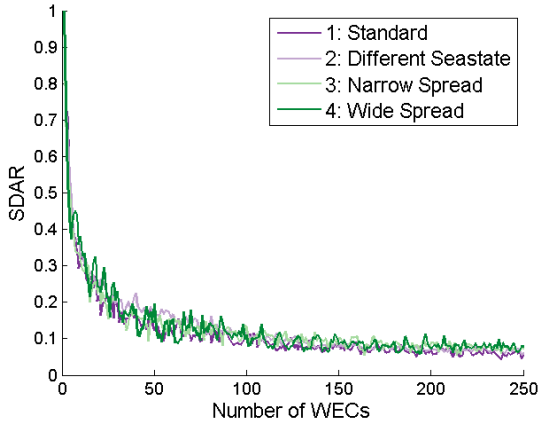

Fig. 13: SDAR's for an array of 2B-PA's concepts

Figures 10-13 show how little influence the different seastates and the wave spreading function have on the SDAR values. Of the 4 different WECs considered; the BBDB, SurfPower and 2B-PA have similar mean SDAR's while RME's flap has slightly higher values. RME's flap has the shortest distance between units within the array (25 m compared to minimum of 100 m for the other WECs) [6]. Additionally, the RME flap only has a single degree of freedom, compared to a minimum of 7 degrees of freedom for the other WECs. It is postulated that either, or both, of these factors could be responsible for the higher SDAR. Detailed investigations into the root cause of the higher SDAR values will occur in future work.

The mean and the standard deviation of the SDAR's are used to produce a fitted power series with the associated mean and bounding standard deviation. The power series is formulated according to equation 3:

$$SDAR = ax\text{^}b \quad (3)$$

where the values of a and b are determined from *Matlab's Curve Fitting Toolbox*. The SDAR values for all the different WECs, the 2 different array sizes and different scenarios are presented in Table IV. For the power series fits, the lowest r-square is 0.940 with a mean of 0.968.

TABLE IV
THE CURVE FITTED SDAR'S

	BBDB	SurfPower		2B-PA		RME	
	@ 50	**@50**	**@250**	**@50**	**@250**	**@50**	**@250**
1	0.137	0.156	0.065	0.135	0.058	0.103	0.088
2	0.139	0.161	0.071	0.159	0.066	0.231	0.117
3	0.113	0.195	*0.102*	0.138	0.068	0.149	0.103
4	0.115	0.125	0.061	0.131	0.068	0.179	0.072
M	**0.126**	**0.159**	**0.075**	**0.141**	**0.065**	**0.165**	**0.095**

The power series curve obtained for the 50 unit BBDB, and the 250 SurfPower and 2B-PA WEC array is presented in Figure 14, showing the mean and bounding standard deviations. The SDAP curves for the RME's flap are shown in Figure 15. Finally, the mean and bounding standard deviation values for the figures are presented in Table V.

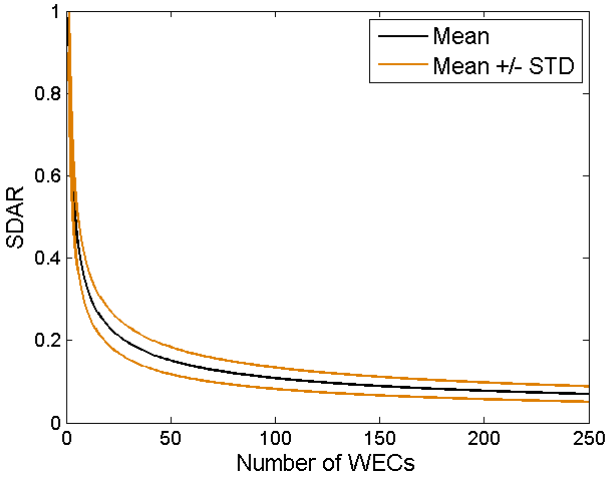

Fig. 14: The mean SDAR for the BBDB, SurfPower and the 2B-PA

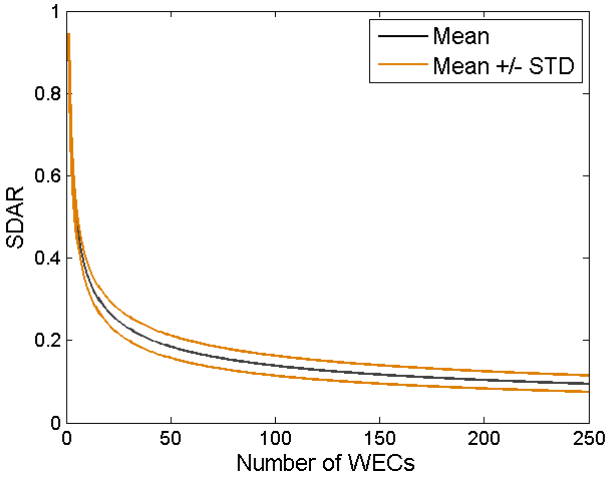

Fig. 15: The mean SDAR for RME's flap

TABLE V
THE POWER SERIES CURVE FITTING PARAMETERS FOR THE MEAN AND MEAN BOUNDED BY THE STANDARD DEVIATION

	BBDB, SurfPower, 2B-PA		RME	
	a	*b*	*a*	*b*
Mean	0.984	-0.479	0.938	-0.416
Mean + std	1.081	-0.453	0.935	-0.380
Mean - std	0.899	-0.520	0.945	-0.459

C. *Frequency domain response*

A Fast Fourier Transform (FFT) was performed on either the simulated 250 (or 50) unit array power, and the power resulting from the multiplication of a single unit power, the array size and the SDAR for that array. The FFT was performed with a Hamming window, using an overlap of half of the window, and taking 11 equally sized samples. The results are presented in Figures 16-19.

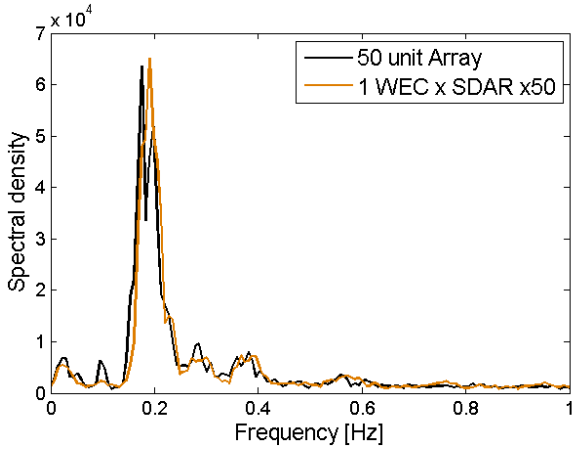

Fig. 16: Frequency domain response of a single unit and array of BBDB

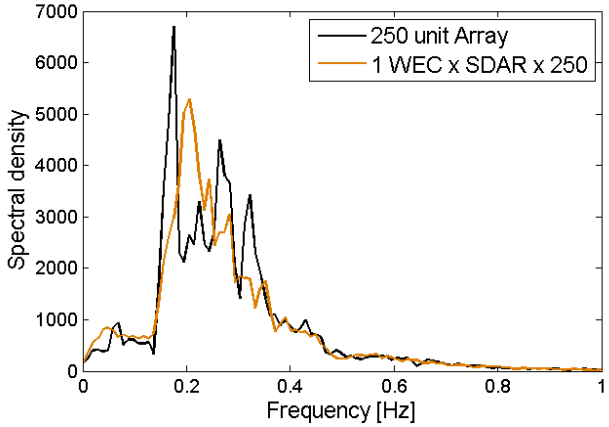

Fig. 17: Frequency domain response of a single unit and array of RME's flaps

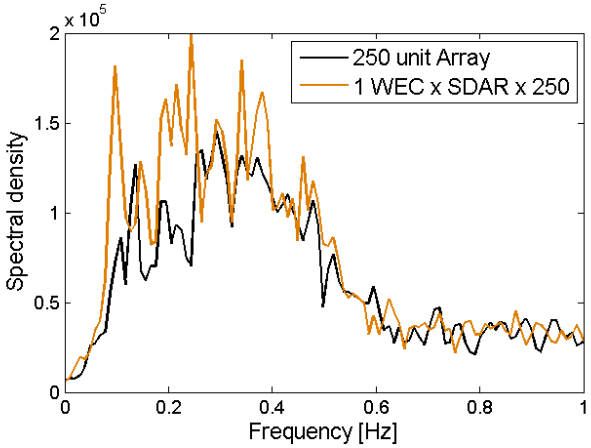

Fig. 18: Frequency domain response of a single unit and array of SurfPower's

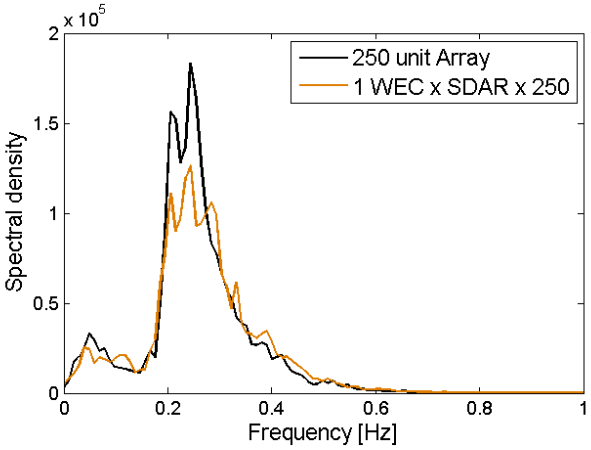

Fig. 19: Frequency domain response of a single unit and array of 2B-PAs.

The similarity in the frequency response signals is immediately evident. The difference between the two curves was determined by normalizing both curves by the maximum array power spectral density. The mean of the absolute bias, for values up to 1 Hz, are presented in Table VI. It is clear from Figures 16-19, and an average bias of 5.64% from Table VI, that the frequency response of the power from the simulated array and from a single WEC has only minor differences. The characteristic frequency response and magnitudes are similar enough to provide confidence in using them for the stochastic model.

TABLE VI
THE MEAN OF THE NORMALIZED ABSOLUTE BIAS OF THE FREQUENCY DOMAIN RESPONSE, UP TO 1 HZ

	BBDB	RME		SurfPower		2B-PA	
	@ 50	@50	@250	@50	@250	@50	@250
	[%]	[%]	[%]	[%]	[%]	[%]	[%]
1	2.45	4.02	4.34	9.16	8.44	3.31	5.19
2	2.90	5.35	4.90	7.27	14.97	4.13	3.15
3	3.01	4.22	4.33	7.80	8.68	5.78	6.13
4	2.49	9.46	11.89	2.55	2.78	4.40	4.84
M	**2.71**	**5.76**	**6.36**	**6.69**	**8.72**	**4.41**	**4.83**

IV. STOCHASTIC MODEL

The stochastic model of the array power was built using detailed knowledge about a single WECs' power extracted and the associated SDAR value. Using the power series parameters presented in Table V, the mean SDAR can be calculated for any size of array.

The stochastic model of the array power is calculated by:

1) Finding the difference for adjacent terms of the power series for a single WEC. This produces a zero averaged power signal

2) Performing an FFT on this zero averaged power from a single WEC.

3) Multiplying the complex FFT signal by the SDAR, the number of units in the array and $\sqrt{2}$.

4) The magnitudes of this complex signal are obtained and retained. The phase of this signal is discarded.
5) Random phases between 0 and 2π are generated and multiplied by the imaginary number, i.
6) The magnitude of the original signal is multiplied by the exponential of the newly generated phases. This generates a new signal of complex numbers that has the same magnitude as the signal of step 4 but randomly assigned phases.
7) The Inverse Fourier transform is implemented on the result of step 6. Steps 1 through 7 are presented in Equation 4.

$$\Delta P_j^* = \mathcal{F}^{-1}\left(\left|\mathcal{F}(\Delta p_j).\sqrt{2}\,.SDAR\,.U\right| \times \exp(i\,\phi_j)\right) \quad (4)$$

where Δ is the difference between adjacent terms in the time series, P_j* is the variation in the array power, p_j is the power of a single unit, U is the number of units in the array and φ_j are the randomly generated phases
8) The cumulative sum of the output of step 7 is added to the product of the mean power from a single WEC and the number of WECs in the array (see Equation 5).

$$P_j = U\bar{p} + \sum_{k=1}^{j} \Delta P_k^* \quad (5)$$

where P_j is the stochastic array power and $\bar{p}$ is the mean power of a single WEC.

The fundamental assumption being made is that the power recovered is composed of a number of frequency components that are statistically orthogonal, similar in concept, to the work of [23].

Figures 20-23 plot the power from the simulated 50 or 250 WEC array against the results of the stochastic model, created using only one WEC simulation and the values in Table V. The similarity between the stochastic model and the simulated array power is immediately observed. The frequency response of the stochastic model signal is the same as the frequency response of the simulated array and the single WEC presented in Figures 16-19. For clarity, the mean of the stochastic model is kept constant with the simulated array mean in Figures 20-23. Given that we are primarily interested in the variation in the array power, rather than the differences in mean power recovered, this allows for easier comparison.

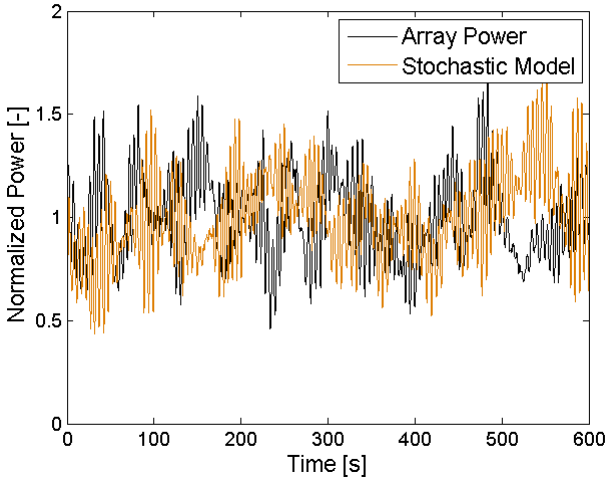

Fig. 20: The actual and stochastic model of the array power for the BBDB

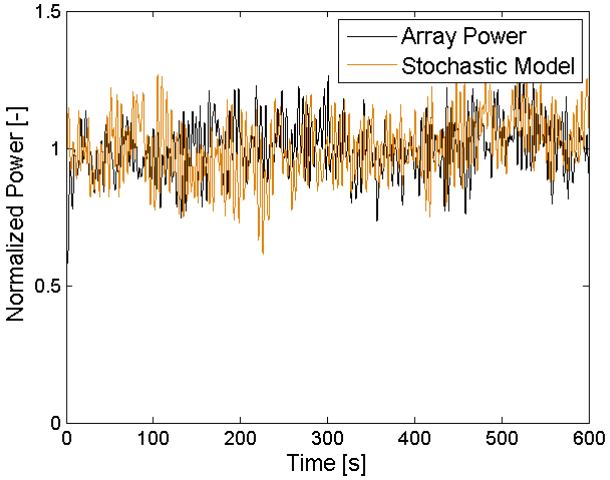

Fig.21: The actual and stochastic model of the array power for the RME flap

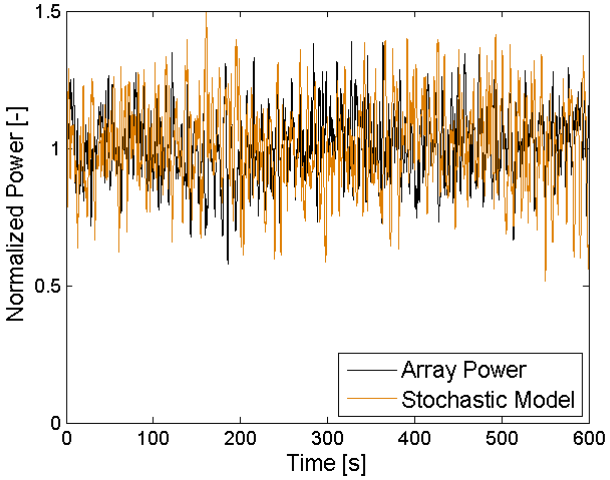

Fig. 22: The actual and stochastic model of the array power for SurfPower

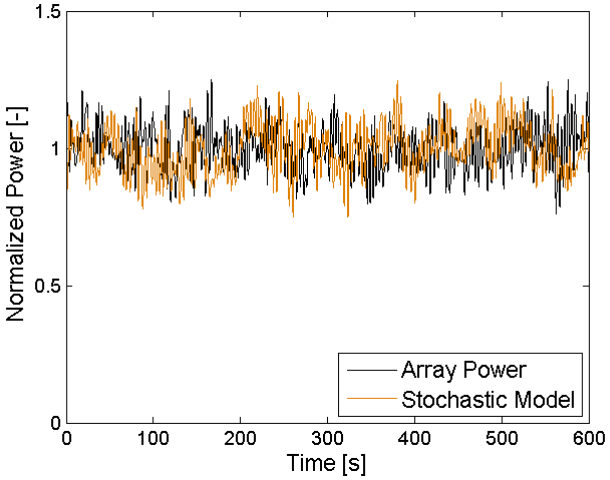

Fig. 23: The actual and stochastic model of the array power for the 2B-PA concept

If the SDAR for the array is not known, the mean value can be calculated from Table V for any size of array, assuming a multi degree of freedom WEC with array spacing of at least

TABLE VII
THE 60 SECOND AND 0.2 SECOND RELATIVE MAXIMUM POWER, FOR THE SIMULATED (SIM) AND STOCHASTIC (STOCH) MODELS

		BBDB		RME				SurfPower				2B-PA			
		50 WECs		50 WECs		250 WECs		50 WECs		250 WECs		50 WECs		250 WECs	
		Sim.	Stoch.	Sim.	Stoch.	Sim.	Stoch.	Sim.	Stoch.	Sim.	Stoch.	Sim.	Stoch.	Sim.	Stoch.
60 s max power	**1**	1.120	1.143	1.145	1.472	1.062	1.123	1.096	1.189	1.063	1.024	1.081	1.099	1.061	1.237
	2	1.207	1.235	1.122	1.103	1.017	1.090	1.181	1.105	1.057	1.329	1.102	1.050	1.058	1.133
	3	1.079	1.064	1.076	1.154	1.024	1.129	1.159	1.073	1.061	1.027	1.141	1.109	1.093	1.099
	4	1.108	1.228	1.098	1.078	1.029	1.019	1.138	1.059	1.037	1.041	1.075	1.172	1.037	1.072
	M	**1.129**	**1.168**	**1.110**	**1.202**	**1.033**	**1.090**	**1.144**	**1.107**	**1.054**	**1.105**	**1.100**	**1.108**	**1.062**	**1.135**
0.2 s max power	**1**	1.654	1.671	1.726	2.099	1.346	1.308	2.252	2.516	1.387	1.549	1.741	1.615	1.252	1.484
	2	1.776	1.610	1.856	2.026	1.306	1.390	2.901	2.446	1.585	1.753	1.892	1.740	1.310	1.420
	3	1.397	1.383	1.988	1.804	1.361	1.410	2.177	2.264	1.260	1.460	1.625	1.515	1.332	1.317
	4	1.448	1.576	1.789	1.734	1.290	1.405	2.079	2.078	1.459	1.535	1.904	1.538	1.289	1.286
	M	**1.569**	**1.560**	**1.840**	**1.916**	**1.326**	**1.378**	**2.352**	**2.326**	**1.423**	**1.574**	**1.791**	**1.602**	**1.296**	**1.377**

100 m. For a 250 unit array, this calculation would produce array power predictions that have a 95% confidence that the SDAR was within 0.038 and the frequency domain response would have a likely error of the mean of the normalized absolute bias of 5.64%.

A. *Power Quality*

A measure of the power quality of a signal is determined by its 60 s maximum power (P_{60}) and its 0.2 s maximum power ($P_{0.2}$). This is the maximum of the means of each 60 s or 0.2 s segment of data [24]. In Table VII, we compare the performance of the stochastic model and the fully simulated WEC array. Table VII shows the P_{60} and $P_{0.2}$ results, normalized by the mean array power, for all the different WECs and array sizes tested. The mean percentage difference between the stochastic and simulated 50 unit WEC arrays is 6.2% for P_{60} and 8.6% for $P_{0.2}$; for the 250 unit WEC array it is 6.6% for P_{60} and 7.4% for $P_{0.2}$.

V. DISCUSSION

This study has illustrated that the SDAR for an array of WECs is relatively consistent regardless of WEC architecture; with the potential exception of WECs that are closely spaced and/or have limited degrees of freedom. The SDAR has a power series relationship with the number of WECs within the array. The frequency domain response of the power from a single WEC and an array of multiple WECs are similar in relative magnitude. These factors have allowed us to build a stochastic model of a WEC array, using only information from a single WEC power output.

In this work, there has been no inclusion of the effects of the WECs on the surrounding wave field, and the resulting change in the wave field due to other WECs. The amplitude of the waves would be affected by these effects; potentially increasing the power recovered in the first row and reducing it for the rows furthest from the incident wave direction, with an expected overall reduction in power absorbed [25]. However, the authors postulate that the variability of the power would decrease when the WECs are subjected to wave fields that are affected by the presence of other WECs. Therefore, the final array power, although smaller in magnitude, may be smoother. The variability of the power from this stochastic model is the likely typical worst case scenario, when no interactions between the different WECs are affecting the wave field.

If a WEC has a problematic frequency response, for example frequencies that lead to flicker [26], then the frequencies are still likely to be present in the power output for an array, although their magnitude will be much reduced. These problematic frequencies would still need to be filtered; yet filtering the lower magnitude array power may be easier and cheaper than filtering individual WEC power outputs.

It should be noted that care has to be taken when using the mean power, from a single simulation run, to predict the mean power of a WEC array. As demonstrated in Figure 24, there is variation in the mean power obtained from any single WEC, for the same sea-state, due to the influence of the wave-wave interactions, so averaging multiple runs is suggested.

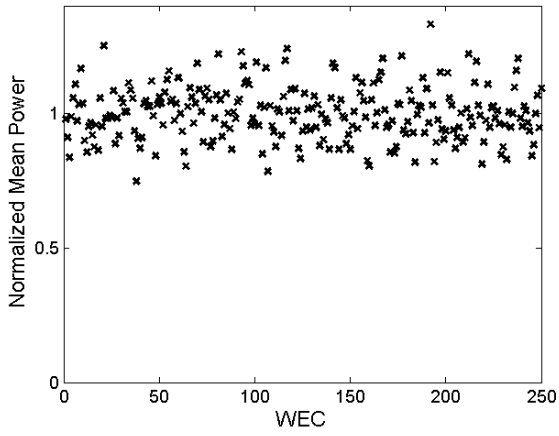

Fig. 24: The mean power output from each 2B-PA WEC in the same array

VI. Conclusions

This paper has presented a novel method to accurately predict the temporal variation of the power production from WEC arrays, using only detailed knowledge of a single WEC device. Through a time and frequency domain analysis of 4 different WEC architectures, including a series of different sea-states and direction spreading functions, a stochastic model was developed. The stochastic model provides WEC array power estimates in a significantly more computationally efficient method than modelling all WEC's within an array.

A newly presented measure to represent the difference between the variation in the array power and a single WEC power is the SDAR (Standard Deviation Array Ratio). The SDAR is the ratio of the standard deviation of the power of an array and the standard deviation of power from a single unit multiplied the number of units in the current array. The SDAR is shown to be insensitive to sea-state conditions, wave directional spread, and the type of WEC (for the majority of WECs tested). It is postulated that for WECs with multiple degrees of freedom, and with a minimum spacing of 100 m, that the SDAR may be insensitive to WEC architecture.

The presented stochastic model of any WEC array can be built from using knowledge of only the SDAR and a single units power output. The SDAR for a 250 unit array, with the above DOF and spacing conditions, has a mean of 0.070 and a ±0.038, 95% confidence interval. The frequency domain difference between a stochastic model of the array power and the actual array power from individually modelled WECs has an average 5.64% difference in the absolute normalized bias.

The power quality from the WEC arrays was quantified using the maximum of the average power over 60 s (P_{60}) and over 0.2 s ($P_{0.2}$). The mean percentage difference between the simulated and stochastic models for the array power from 50 WEC arrays is just 6.2% for P_{60} and 8.6% for $P_{0.2}$; for the 250 WEC array it is 6.6% for P_{60} and 7.4% for $P_{0.2}$.

This work does not account for the wave field being affected by the presence of other WECs in the array. The presence of other WECs affecting the wave field will likely decrease the array power recovered and reduce the variability of the array power. Therefore, the power variability from the stochastic model can be considered to be a typical worst-case scenario.

This stochastic model will be valuable to grid integration studies by allowing for a computationally and financially efficient method of predicting the power variability from utility scale WEC arrays. Given that only information about the power from a single WEC is required, this method will significantly reduce the efforts and complexity required to better understand WEC array power production.

References

[1] J. Tissandier, A. Babarit, and A. H. Clément, "Study of the smoothing effect on the power production in an array of SEAREV wave energy converters," in *Proceedings of the 18th ISOPE*, 2008, vol. 8, pp. 374–381.

[2] M. Rahm, O. Svensson, C. Boström, R. Waters, and M. Leijon, "Experimental results from the operation of aggregated wave energy converters," *IET Renew. Power Gener.*, vol. 6, no. November 2011, p. 149, 2012.

[3] J. Sjolte, G. Tjensvoll, and M. Molinas, "Power Collection from Wave Energy Farms," *Appl. Sci.*, vol. 3, pp. 420–436, 2013.

[4] J. Engström, M. Eriksson, M. Göteman, J. Isberg, and M. Leijon, "Performance of large arrays of point absorbing direct-driven wave energy converters," *J. Appl. Phys.*, vol. 114, no. 2013, 2013.

[5] J. Aubry, P. Bydlowski, B. Multon, H. Ben Ahmed, and B. Borgarino, "Energy Storage System Sizing for Smoothing Power Generation of Direct Wave Energy Converters," *Proc. 3rd Int. Conf. Ocean Energy (ICOE 2010)*, pp. 1–7, 2010.

[6] F. Ueckerdt, L. Hirth, G. Luderer, and O. Edenhofer, "System LCOE: What are the costs of variable renewables?," *Energy*, vol. 63, pp. 61–75, 2013.

[7] D. Bull and P. Jacob, "Methodology for creating nonaxisymmetric WECs to screen mooring designs using a Morison Equation approach," in *Oceans*, 2012, pp. 1–9.

[8] C. Smith, D. Bull, S. Willits, and F. Arnold, "Optimization and Annual Average Power Predictions of a Backward Bent Duct Buoy Oscillating Water Column Device Using the Wells Turbine," *7th Annu. Glob. Mar. …*, pp. 1–10, 2014.

[9] H. Bailey, B. Robertson, and B. J. Buckham;, "Wave-to-Wire Simulation of a Floating Oscillating Water Column Wave Energy Converter," *In prep*.

[10] E. Ramudu, "Ocean wave energy-driven desalination systems for off-grid coastal communities in developing countries," *Proc. - 2011 IEEE Glob. Humanit. Technol. Conf. GHTC 2011*, pp. 287–289, 2011.

[11] H. Bailey, J. Ortiz, B. Robertson, B. Buckham, and R. Nicoll, "A Methodology for Wave-To-Wire WEC simulations," in *Marine Renewable Energy Technology Symposium (METS2014)*, 2014.

[12] H. Bailey, B. Robertson, and B. J. Buckham, "Optimizing wecs for canadian waters," in *Int. Conf. Ocean Energy (ICOE 2014)*, 2014.

[13] R. Nicoll, C. Wood, and A. Roy, "Comparison of physical model tests with a time domain simulation model of a wave energy converter," *ASME 2012 …*, pp. 1–10, 2012.

[14] S. J. Beatty, B. J. Buckham, and P. Wild, "Modeling , Design and Testing of a Two-Body Heaving Wave Energy Converter," in *Int. Soc. Offshore & Polar Eng. (ISOPE)*, 2007.

[15] J. P. Ortiz, H. Bailey, B. Buckham, and C. Crawford, "Surrogate Based Design of a Mooring System for a Self-reacting Point Absorber," in *Int. Soc. Offshore & Polar Eng. (ISOPE)*, 2015.

[16] J. Falnes, *Ocean Waves and Oscillating Systems: linear interactions including wave-energy extraction*. Cambridge University Press, 2002.

[17] B. J. Buckham, "Dynamics modelling of low-tension tethers for submerged remotely operated vehicles," University of Victoria, 2003.

[18] Dynamic Systems Analysis Ltd, *ProteusDS 2013 Manual*. Solver 2.2.1977, 2013.

[19] A. Babarit, "On the park effect in arrays of oscillating wave energy converters," *Renew. Energy*, vol. 58, pp. 68–78, 2013.

[20] B. Robertson, C. Hiles, E. Luzko, and B. Buckham, "Quantifying the Wave Energy Resource and Farm Siting Opportunities for Western Canada," in *Int. Conf. Ocean Energy (ICOE 2014)*, 2014, vol. 1, no. 250.

[21] B. R. D. Robertson, C. E. Hiles, and B. J. Buckham, "Characterizing the near shore wave energy resource on the west coast of Vancouver Island, Canada," *Renew. Energy*, vol. 71, pp. 665–678, Nov. 2014.

[22] DNV, *Recommended practice DNV-RP-C205 environmental conditions and environmental loads*. 2010, p. Table 3–1.

[23] M. Folley and T. Whittaker, "Spectral modelling of wave energy converters," *Coast. Eng.*, vol. 57, pp. 892–897, 2010.

[24] "Measurement and Assessment of Power Quality Characteristics of Grid Connected Wind Turbines—Part 21. IEC Standard," 61400-21, 2008.

[25] B. Borgarino, A. Babarit, and P. Ferrant, "Impact of wave interactions effects on energy absorption in large arrays of wave energy converters," *Ocean Eng.*, vol. 41, pp. 79–88, 2012.

[26] A. Blavette, D. L. O'Sullivan, R. Alcorn, T. W. Lewis, and M. G. Egan, "Impact of a medium-size wave farm on grids of different strength levels," *IEEE Trans. Power Syst.*, vol. 29, no. 2, pp. 917–923, 2014.